Anytime Sampling for Autoregressive Models via Ordered Autoencoding

Anonymous Author(s)
Affiliation
Address
email

Abstract

Autoregressive models are widely used for tasks such as image and audio generation. Sampling from autoregressive models, however, can be slow, involving a computation that is sequential in nature and typically scales linearly with respect to the data dimension. To address this difficulty, we propose a new family of autoregressive models that enables anytime sampling. Inspired by Principal Component Analysis (PCA), we learn a structured representation space where dimensions are ordered based on their importance with respect to reconstruction. Using an autoregressive model in this latent space, we trade off sample quality for computational efficiency by truncating the generation process before decoding into the original data space. Experimentally, we demonstrate in several image and audio generation tasks that sample quality degrades gracefully as we reduce the computational budget for sampling. The approach suffers almost no loss in sample quality (measured by FID) using only 60% to 80% of all latent dimensions for image data.

1 Introduction

Autoregressive models are a prominent approach to data generation, and have been widely used to produce high quality samples of images (Oord et al., 2016b; Salimans et al., 2017; Menick & Kalchbrenner, 2018), audio (Oord et al., 2016a), video (Kalchbrenner et al., 2017) and text (Kalchbrenner et al., 2016; Radford et al., 2019). These models represent a joint distribution as a product of (simpler) conditionals, and sampling requires iterating over all these conditional distributions in a certain order. As a result, the sampling process of autoregressive models can be slow. Due to the sequential nature of this process, the computational cost will grow at least linearly with respect to the number of conditional distributions, which is typically equal to the data dimension.

Although caching techniques have been developed to speed up generation (Ramachandran et al., 2017; Guo et al., 2017), the high cost of sampling limits their applicability in many scenarios. For example, when running on multiple devices with different computational resources, we may wish to trade off sample quality for faster generation based on the computing power available on each device. Currently, a separate model must be trained for each device (*i.e.*, computational budget) in order to trade off sample quality for faster generation, and there is no way to control this trade-off on the fly to accommodate instantaneous resource availability at time-of-deployment.

To address this difficulty, we consider the novel task of *adaptive* autoregressive generation under *computational constraints*. We seek to build a *single model* that can automatically trade-off sample quality versus computational cost via *anytime sampling*, *i.e.*, where the sampling process may be terminated anytime (*e.g.*, because of exhausted computational budget) to yield a *complete* sample whose sample quality decays with the earliness of termination.

Submitted to 34th Conference on Neural Information Processing Systems (NeurIPS 2020). Do not distribute.

In particular, we take advantage of a generalization of Principal Components Analysis (PCA) proposed by Rippel et al. (2014), which learns an ordered representations induced by a structured application of dropout to the representations learned by an autoencoder. Such a representation encodes raw data into a latent space where dimensions are sorted based on their importance for reconstruction. Autoregressive modeling is then applied in the ordered representation space instead. This approach enables a natural trade-off between quality and computation by truncating the length of the representations: When running on devices with high computational capacity, we can afford to generate the full representation and decode it to obtain a high quality sample; when on a tighter computational budget, we can generate only the first few dimensions of the representation and decode it to a sample whose quality degrades smoothly with truncation. Because decoding is usually fast and the main computation bottleneck lies on the autoregressive part, the run-time grows proportionally relative to the number of sampled latent dimensions.

Through experiments, we show that our autoregerssive models are capable of trading off sample quality and inference speed. When training autoregressive models on the latent space given by our encoder, we witness little degradation of image sample quality using only around 60% to 80% of all latent codes, as measured by Fréchet Inception Distance (Heusel et al., 2017b) on CIFAR-10 and CelebA. Compared to standard autoregressive models, our approach allows the sample quality to degrade gracefully as we reduce the computational budget for sampling. We also observe that on the VCTK audio dataset (Veaux et al., 2017), our autoregressive model is able to generate the low frequency features first, then gradually refine the waveforms with higher frequency components as we increase the number of sampled latent dimensions.

2 Background

Autoregressive Models Autoregressive models define a probability distribution over data points $\mathbf{x} \in \mathbb{R}^D$ by factorizing the joint probability distribution as a product of univariate conditional distributions with the chain rule. Using p_θ to denote the distribution of the model, we have:

$$p_\theta(\mathbf{x}) = \prod_{i=1}^{D} p_\theta(x_i \mid x_1, \cdots, x_{i-1}) \tag{1}$$

The model is trained by maximizing the likelihood:

$$\mathcal{L} = \mathbb{E}_{p_d(\mathbf{x})}[\log p_\theta(\mathbf{x})], \tag{2}$$

where $p_d(\mathbf{x})$ represents the data distribution.

Different autoregressive models adopt different orderings of input dimensions and parameterize the conditional probability $p_\theta(x_i \mid x_1, \cdots, x_{i-1}), i = 1, \cdots, D$ in different ways. Most architectures over images order the variables $x_1, \cdots, x_D$ of image $\mathbf{x}$ in *raster scan order* (*i.e.*, left-to-right then top-to-bottom). Popular autoregressive architectures include MADE (Papamakarios et al., 2017), PixelCNN (Oord et al., 2016b; van den Oord et al., 2016; Salimans et al., 2017) and Transformer (Vaswani et al., 2017), where they respectively use masked linear layers, convolutional layers and self-attention blocks to ensure that the output corresponding to $p_\theta(x_i \mid x_1, \cdots, x_{i-1})$ is oblivious of $x_i, x_{i+1}, \cdots, x_D$.

Cost of Sampling During training, we can evaluate autoregressive models efficiently because $x_1, \cdots, x_D$ are provided by data and all conditionals $p(x_i \mid x_1, \cdots, x_{i-1})$ can be computed in parallel. In contrast, sampling from autoregressive models is an inherently sequential process and cannot be easily accelerated by parallel computing: we first need to sample x_1, after which we sample x_2 from $p_\theta(x_2 \mid x_1)$ and so on—the i-th variable x_i can only be obtained after we have already computed $x_1, \cdots, x_{i-1}$. Thus, the run-time of autoregressive generation grows *at least linearly* with respect to the length of a sample. In practice, the sample length D can be more than hundreds of thousands for real-world image and audio data. This poses a major challenge to fast autoregressive generation on a small computing budget.

3 Anytime Sampling with Ordered Autoencoders

Our goal is to circumvent this linear time complexity of autoregressive models by pushing the task of autoregressive modeling from the original data space (e.g., pixel space) into an ordered representation

space. In doing so, we develop a new class of autoregressive models where premature truncation of the autoregressive sampling process leads to the generation of a *lower quality* sample instead of an *incomplete* sample. In this section, we shall first describe the learning of the ordered representation space via the use of an *ordered autoencoder*. We then describe how to achieve anytime sampling with ordered autoencoders.

3.1 Ordered Autoencoders

Consider an autoencoder that encodes an input $\mathbf{x} \in \mathbb{R}^D$ to a code $\mathbf{z} \in \mathbb{R}^K$. Let $\mathbf{z} = e_\theta(\mathbf{x}) : \mathbb{R}^D \to \mathbb{R}^K$ be the encoder parameterized by θ and $\mathbf{x}' = d_\phi(\mathbf{z}) : \mathbb{R}^K \to \mathbb{R}^D$ be the decoder parameterized by ϕ. We define $e_\theta(\cdot)_{\leq i} : \mathbf{x} \in \mathbb{R}^D \mapsto (z_1, z_2, \cdots, z_i, 0, \cdots, 0)^\mathsf{T} \in \mathbb{R}^K$, which truncates the representation to the first i dimensions of the encoding $\mathbf{z} = e_\theta(\mathbf{x})$, masking out the remainder of the dimensions with a zero value. We define the ordered autoencoder objective as

$$\frac{1}{N}\sum_{i=1}^{N}\frac{1}{K}\sum_{j=1}^{K}\|\mathbf{x}_i - d_\phi(e_\theta(\mathbf{x}_i)_{\leq j})\|_2^2 . \tag{3}$$

We note that Eq. (3) is equivalent to Rippel et al. (2014)'s nested dropout formulation using a uniform sampling of possible truncations. Moreover, when the encoder/decoder pair is constrained to be a pair of orthogonal matrices up to a transpose, then the optimal solution in Eq. (3) recovers PCA.

3.1.1 Theoretical Analysis

Rippel et al. (2014)'s analysis of the ordered autoencoder is limited to linear/sigmoid encoder and a linear decoder. In this section, we extend the analysis to general autoencoder architectures by employing an information-theoretic framework to analyze the importance of the i-th latent code to reconstruction for ordered autoencoders. We first reframe our problem from a probabilistic perspective. In lieu of using deterministic autoencoders, we assume that both the encoder and decoder are stochastic functions. In particular, we let $q_{e_\theta}(\mathbf{z} \mid \mathbf{x})$ be a probability distribution over $\mathbf{z} \in \mathbb{R}^K$ conditioned on input $\mathbf{x}$, and similarly let $p_{d_\phi}(\mathbf{x} \mid \mathbf{z})$ be the stochastic counterpart to $d_\phi(\mathbf{z})$. We then use $q_{e_\theta}(\mathbf{z} \mid \mathbf{x})_{\leq i}$ to denote the distribution of $(z_1, z_2, \cdots, z_i, 0, \cdots, 0)^\mathsf{T} \in \mathbb{R}^K$, where $\mathbf{z} \sim q_{e_\theta}(\mathbf{z} \mid \mathbf{x})$, and let $p_{d_\phi}(\mathbf{x} \mid \mathbf{z})_{\leq i}$ represent the distribution of $p_{d_\phi}(\mathbf{x} \mid (z_1, z_2, \cdots, z_i, 0, \cdots, 0)^\mathsf{T} \in \mathbb{R}^K)$. We can modify Eq. (3) to have the following form:

$$\mathbb{E}_{x\sim p_d(\mathbf{x}), i\sim\mathcal{U}\{1,K\}}\mathbb{E}_{\mathbf{z}\sim q_{e_\theta}(\mathbf{z}|\mathbf{x})_{\leq i}}[-\log p_{d_\phi}(\mathbf{x}|\mathbf{z})_{\leq i}], \tag{4}$$

where $\mathcal{U}\{1, K\}$ denotes a uniform distribution over $\{1, 2, \cdots, K\}$, and $p_d(\mathbf{x})$ represents the data distribution. We can choose both the encoder and decoder to be fully factorized Gaussian distributions with a fixed variance σ^2, then Eq. (4) can be simplified to

$$\mathbb{E}_{p_d(\mathbf{x})}\left[\frac{1}{K}\sum_{i=1}^{K}\mathbb{E}_{\mathbf{z}\sim\mathcal{N}(e_\theta(\mathbf{x})_{\leq i};\sigma^2)}\left[\frac{1}{2\sigma^2}\|\mathbf{x} - d_\phi(\mathbf{z})_{\leq i}\|_2^2\right]\right].$$

The stochastic encoder and decoder in this case will become deterministic when $\sigma \to 0$, and the above equation will yield the same encoder/decoder pair as Eq. (3) when $\sigma \to 0$ and $N \to \infty$.

The optimal encoders and decoders that minimize Eq. (4) satisfy the following property.

Theorem 1. *Let $\mathbf{x}$ denote the input random variable. Assuming both the encoder and decoder are optimal in terms of minimizing Eq. (4), and $\forall i \in 2, \cdots, K$, $z_{i-1} \perp z_i \mid \mathbf{x}$, we have*

$$\forall i \in \{2, \cdots, K\} : \; I(z_i; \mathbf{x}|z_{\leq i-1}) \leq I(z_{i-1}; \mathbf{x}|z_{\leq i-2}),$$

where $z_{\leq i}$ denotes $(z_1, z_2, \cdots, z_i)$.

We defer the proof to Appendix A.1. The assumption $z_{i-1} \perp z_i \mid \mathbf{x}$ holds whenever the encoder $q_\theta(\mathbf{z} \mid \mathbf{x})$ is a factorized distribution, which is a common choice in variational autoencoders (Kingma & Welling, 2013), and we use $I(\mathbf{a}; \mathbf{b} \mid \mathbf{c})$ to denote the mutual information between random variables $\mathbf{a}$ and $\mathbf{b}$ conditioned on $\mathbf{c}$. Intuitively, the above theorem states that for optimal encoders and decoders that minimize Eq. (4), one can extract less additional information about the raw input as the code gets longer. Therefore, there exists a natural ordering among different dimensions of the code based on the additional information they can provide for reconstructing the inputs.

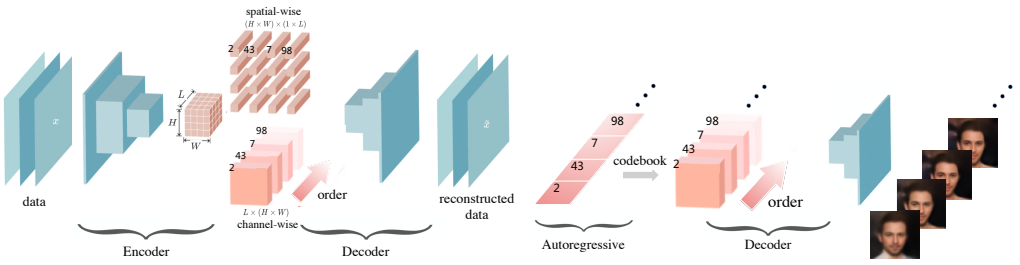

(a) (b)

Figure 1: **(a)** Spatial-wise quantization vs. channel-wise quantization. **(b)** Anytime sampling for OVQ-VAE.

3.2 Anytime Sampling

Once we have learned an ordered autoencoder, we then train an autoregressive model on the full length codes in the ordered representation space, to adopt the ex-post density estimation Ghosh et al. (2020). For each input $\mathbf{x}_i$ in a dataset $\mathbf{x}_1, \cdots, \mathbf{x}_N$, we feed it to the encoder to get $\mathbf{z}_i = e_\theta(\mathbf{x}_i)$. The resulting codes $\mathbf{z}_1, \mathbf{z}_2, \cdots, \mathbf{z}_N$ are used as training data. After training both the ordered autoencoder and autoregressive model, we can perform anytime sampling on a large spectrum of computing budgets. Suppose for example we can afford to generate T code dimensions from the autoregressive model, denoted as $\mathbf{z}_{\leq T} \in \mathbb{R}^T$. We can simply zero-pad it to get $(z_1, z_2, \cdots, z_T, 0, \cdots, 0)^\intercal \in \mathbb{R}^K$ and decode it to get a complete sample. Unlike the autoregressive part, the decoder has access to all dimensions of the latent code at the same time and can decode in parallel. On modern GPUs, the code length has minimal effect on the run-time of decoding, as long as the decoder is not itself autoregressive (see empirical verifications in Section 5.2.2).

4 Ordered VQ-VAE

In this section, we apply the ordered autoencoder framework to the vector quantized variational autoencoder (VQ-VAE) and its extension (van den Oord et al., 2017; Razavi et al., 2019). Since these models are quantized autoencoders paired with a latent autoregressive model, they admit a natural extension to *ordered* VQ-VAEs (OVQ-VAEs) under our framework—a new family of VQ-VAE models capable of anytime sampling. Below, we begin by describing the VQ-VAE, and then highlight two key design choices (ordered discrete codes and channel-wise quantization) critical for OVQ-VAEs.

4.1 VQ-VAE

To construct a VQ-VAE with code length of K discrete latent variables , the encoder must first map the raw input $\mathbf{x}$ to a continuous representation $\mathbf{z}_e = e_\theta(\mathbf{x}) \in \mathbb{R}^{K \times D}$, before feeding it to a vector-valued quantization function $q : \mathbb{R}^{K \times D} \to \{1, 2, \cdots, C\}^K$ defined as

$$q(\mathbf{z}_e)_j = \underset{i \in \{1, \cdots, C\}}{\arg\min} \left\| \mathbf{e}_i - \mathbf{z}_{e,j} \right\|_2 ,$$

where $q(\mathbf{z}_e)_j \in \{1, 2, \cdots, C\}$ denotes the j-th component of the vector-valued function $q(\mathbf{z}_e)$, $\mathbf{z}_{e,j} \in \mathbb{R}^D$ denotes the j-th row of $\mathbf{z}_e$, and $\mathbf{e}_i$ denotes the i-th row of the embedding matrix $\mathbf{E} \in \mathbb{E}^{C \times D}$. Next, we view $q(\mathbf{z}_e)$ as a sequence of indices and use them to look up embedding vectors from the codebook $\mathbf{E}$. This yields a latent representation $\mathbf{z}_d \in \mathbb{R}^{K \times D}$, given by $\mathbf{z}_{d,j} = \mathbf{e}_{q(\mathbf{z}_e)_j}$, where $\mathbf{z}_{d,j} \in \mathbb{R}^D$ denotes the j-th row of $\mathbf{z}_d$. Finally, we can decode $\mathbf{z}_d$ to obtain the reconstruction $d_\phi(\mathbf{z}_d)$. This procedure can be viewed as a regular autoencoder with a non-differentiable nonlinear function that maps each latent vector $\mathbf{z}_{e,j}$ to 1-of-K embedding vectors $\mathbf{e}_i$.

During training, we use the straight-through gradient estimator (Bengio et al., 2013) to propagate gradients through the quantization function, *i.e.*, gradients are directly copied from the decoder input $\mathbf{z}_d$ to the encoder output $\mathbf{z}_e$. The loss function for training on a single data point $\mathbf{x}$ is given by

$$\left\| d_\phi(\mathbf{z}_d) - \mathbf{x} \right\|_2^2 + \left\| \mathrm{sg}[e_\theta(\mathbf{x})] - \mathbf{z}_d \right\|_F^2 + \beta \left\| e_\theta(\mathbf{x}) - \mathrm{sg}[\mathbf{z}_d] \right\|_F^2 , \tag{5}$$

where sg stands for the `stop_gradient` operator, and β is a hyper-parameter ranging from 0.1 to 2.0. The first term of Eq. (5) is the standard reconstruction loss, the second term is for embedding learning while the third term is for training stability (van den Oord et al., 2017). Samples from a VQ-VAE can be produced by first training an autoregressive model on its latent space, followed by decoding samples from the autoregressive model into the raw data space.

4.2 Ordered Discrete Codes

Since the VQ-VAE outputs a sequence of discrete latent codes $q(\mathbf{z}_e)$, we wish to impose an ordering that prioritizes the code dimensions based on importance to reconstruction. In analogy to Eq. (3), we can modify the reconstruction error term in Eq. (5) to learn ordered latent representations. The modified loss function is an order-inducing objective given by

$$\frac{1}{K}\sum_{i=1}^{K}\left[\,\|d_\phi(\mathbf{z}_{d,\leq i})-\mathbf{x}\|_2^2+\|\mathtt{sg}[e_\theta(\mathbf{x})_{\leq i}]-\mathbf{z}_{d,\leq i}\|_F^2+\beta\,\|e_\theta(\mathbf{x})_{\leq i}-\mathtt{sg}[\mathbf{z}_{d,\leq i}]\|_F^2\,\right], \tag{6}$$

where $e_\theta(\mathbf{x})_{\leq i}$ and $\mathbf{z}_{d,\leq i}$ denote the results of keeping the top i rows of $e_\theta(\mathbf{x})$ and $\mathbf{z}_d$ and then masking out the remainder rows with zero vectors. We uniformly sample the masking index $i \sim \mathcal{U}\{1, K\}$ to approximate the average in Eq. (6) when K is large. This results in the learning of ordered discrete latent variables, which can then be paired with a latent autoregressive model for anytime sampling.

4.3 Channel-Wise Quantization

In Section 4.1, we assume the encoder output to be a $K \times D$ matrix (*i.e.*, $\mathbf{z}_e \in \mathbb{R}^{K\times D}$). In practice, the output can have various sizes depending on the encoder network, and we need to reshape it to a two-dimensional matrix. For example, when encoding images, the encoder is typically a 2D convolutional neural network (CNN) whose output is a 3D latent feature map of size $L \times H \times W$. Here L, H, and W stand for the channel, height, and width of the feature maps. We discuss below how the reshaping procedure can significantly impact the performance of anytime sampling and propose a reshaping procedure that facilitates high-performance anytime sampling.

Consider convolutional encoders on image data, where the output feature map has a size of $L\times H\times W$. The most common way of reshaping this 3D feature map, as in van den Oord et al. (2017), is to let $H \times W$ be the code length, and let the number of channels L be the size of embedding vectors, *i.e.*, $K = H \times W$ and $D = L$. We call this pattern *spatial-wise quantization*, as each spatial location in the feature map corresponds to one code dimension and will be quantized separately. Since the code dimensions correspond to spatial locations of the feature map, they encode local features due to a limited receptive field. This is detrimental to anytime sampling, because early dimensions cannot capture the global information needed for reconstructing the entire image. We demonstrate this in Fig. 2, which shows that VQ-VAE with spatial-wise quantization is only able to reconstruct the top rows of an image with $1/4$ of the code length.

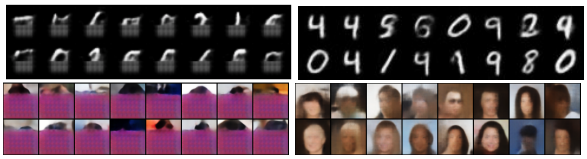

Figure 2: MNIST (**top**) and CelebA (**bottom**) samples generated with $1/4$ of the code length. **Left:** Spatial-wise quantization. **Right:** Channel-wise quantization.

To address this issue, we propose *channel-wise quantization*, where each channel of the feature map is viewed as one code dimension and quantized separately (see Fig. 1(a) for visual comparison of spatial-wise and channel-wise quantization). Specifically, the code length is L (*i.e.*, $K = L$), and the size of the embedding vectors is $H \times W$ (*i.e.*, $D = H \times W$). In this case, one code dimension includes all spatial locations in the feature map and can capture global information better. As shown in the right panel of Fig. 2, channel-wise quantization clearly outperforms spatial-wise quantization for anytime sampling. We use channel-wise quantization in all subsequent experiments.

5 Experiments

In our experiments, we focus on anytime sampling for autoregressive models trained on the latent space of OVQ-VAEs. We first verify that our learning objectives Eq. (3), Eq. (6) are effective at

inducing ordered representations. Next, we demonstrate on several image and audio datasets that our models achieve comparable sample quality to regular VQ-VAEs, while allowing graceful trade-off between sample quality and computation time via anytime sampling. Due to the page limit, we defer the result of audio generation to Appendix B and provide additional experimental details and results in Appendix C and E.

5.1 Ordered Versus Unordered Codes

Our proposed ordered autoencoder framework learns an ordered encoding that is in contrast to the encoding learned by a standard autoencoder (which we shall refer to as unordered). In addition to the theoretical analysis in Section 3.1.1, we provide further empirical analysis to characterize the difference between ordered and unordered codes. In particular, we compare the importance of the i-th code—as measured by the reduction in reconstruction error $\Delta(i)$—for PCA, standard (unordered) VQ-VAE, and ordered VQ-VAE. For VQ-VAE and ordered VQ-VAE, we define the reduction in reconstruction error $\Delta(i)$ for a data point $\mathbf{x}$ as

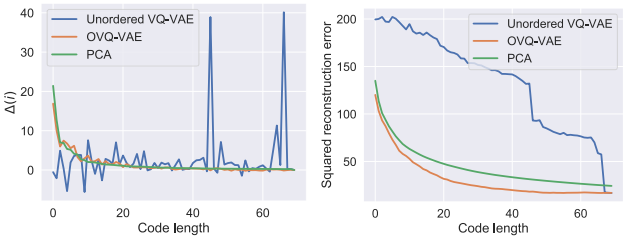

(a) (b)

Figure 3: Ordered vs. unordered codes on CIFAR-10.

$$\Delta_{\mathbf{x}}(i) \triangleq \|d_\phi(\mathbf{z}_{d,\leq i-1}) - \mathbf{x}\|_F^2 - \|d_\phi(\mathbf{z}_{d,\leq i}) - \mathbf{x}\|_F^2 \tag{7}$$

Averaging $\Delta_{\mathbf{x}}(i)$ over the entire dataset thus yields $\Delta(i)$. Similarly we define $\Delta(i)$ as the reduction on reconstruction error of the entire dataset, when adding the i-th principal component for PCA.

Fig. 3(a) shows the $\Delta(i)$'s of the three models on the CIFAR-10. Since PCA and ordered VQ-VAE both learn an ordered encoding, their $\Delta(i)$'s decay gradually as i increases. In contrast, the standard VQ-VAE with an unordered encoding exhibits a highly irregular $\Delta(i)$, indicating no meaningful ordering of the dimensions.

Fig. 3(b) further shows how the reconstruction error decreases as a function of the truncated code length for the three models. Although unordered VQ-VAE and ordered VQ-VAE achieve similar reconstruction errors for sufficiently large code lengths, it is evident that an ordered encoding achieves significantly better reconstructions when the code length is aggressively truncated. When sufficiently truncated, we observe even PCA outperforms unordered VQ-VAE despite the latter being a more expressive model. In contrast, ordered VQ-VAE achieves superior reconstructions compared to PCA and unordered VQ-VAE across all truncation lengths.

5.2 Image Generation

We test the performance of anytime sampling using OVQ-VAEs on several image datasets. We compare our approach to two baselines. One is the original VQ-VAE model proposed by van den Oord et al. (2017) without anytime sampling. The other is using anytime sampling with unordered VQ-VAEs, where the models have the same architectures as ours but are trained by minimizing Eq. (5). We empirically verify that 1) we are able to generate high quality image samples; 2) image quality degrades gracefully as we reduce the sampled code length for anytime sampling; and 3) anytime sampling improves the inference speed compared to naïve sampling of original VQ-VAEs.

We evaluate the model performance on the MNIST, CIFAR-10 (Krizhevsky, 2009) and CelebA (Liu et al., 2014) datasets. For CelebA, the images are resized to 64×64. All pixel values are scaled to the range $[0, 1]$. We borrow the model architectures and optimizers from van den Oord et al. (2017) and adopt some minor modifications. We empirically found that the residual blocks in the original VQ-VAE architecture can lead to unstable training when applying channel-wise quantization, so we replace these residual blocks with convolutional layers, while keeping the number of parameters approximately fixed. The full code length and the codebook size are 16 and 126 for MNIST, 70 and 1000 for CIFAR-10, and 100 and 500 for CelebA respectively. We train a Transformer (Vaswani et al., 2017) on our VQ-VAEs, as opposed to the PixelCNN model used in van den Oord et al. (2017).

Transformers are arguably more suitable for channel-wise quantization, since there are no spatial relations among different code dimensions that can be leveraged by convolutional models (such as PixelCNNs).

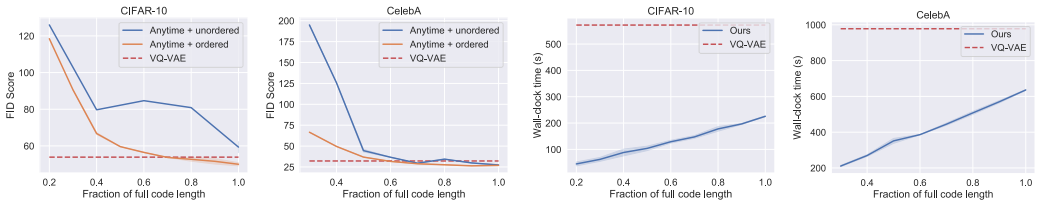

(a) Image quality (b) Inference speed

Figure 4: (a) FID scores for anytime sampling using various code lengths. (b) Inference speed of anytime sampling with different code lengths.

5.2.1 Image Quality

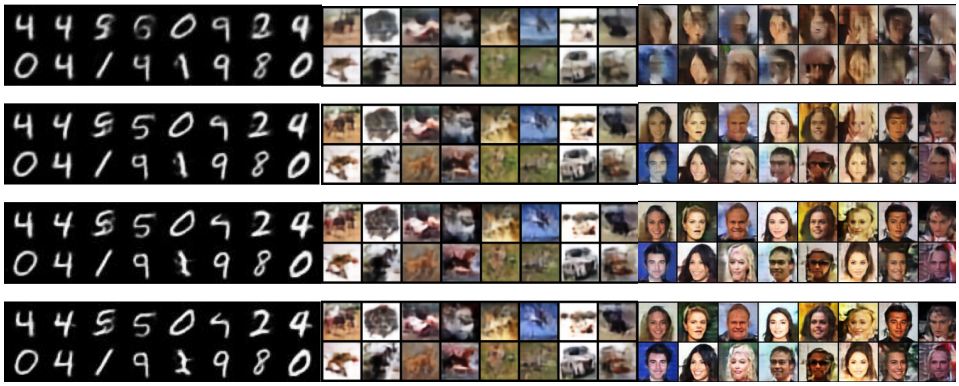

(a) MNIST (b) CIFAR-10 (c) CelebA

Figure 5: Anytime sampling with 0.25/0.5/0.75/1.0 (**top to bottom**) fractions of full code length on MNIST (**left**), CIFAR-10 (**middle**) and CelebA (**right**) datasets.

In Fig. 4(a), we report FID (Heusel et al., 2017b) scores (a popular metric on image quality) on CIFAR-10 and CelebA when performing anytime sampling for ordered versus unordered VQ-VAE. As a reference, we also report the FID scores when using the original VQ-VAE model (with residual blocks and spatial-wise quantization) sampled at the full code length (van den Oord et al., 2017). Our main finding is that OVQ-VAE achieves a better FID score than unordered VQ-VAE at all fractional code lengths (ranging from 20% to 100%); in other words, OVQ-VAE achieves strictly superior anytime sampling performance compared to unordered VQ-VAE on both CIFAR-10 and CelebA.

In Fig. 5 (more in Appendix E.1), we visualize the sample quality degradation as a function of fractional code length when sampling from the OVQ-VAE. We observe a consistent increase in sample quality as we increased the fractional code length. In particular, we observe the model to initially generate a global structure of an image and then gradually fill in local details. We further show in Appendix D that, samples sharing the highest priority latent code have similar global structure.

5.2.2 Inference Speed

We compare the inference speed of our approach vs. the original VQ-VAE model by the wall-clock time needed for sampling. We respectively measure the time of generating 50000 and 100000 images on CIFAR-10 and CelebA datasets, with a batch size of 100. All samples are produced on a single NVIDIA TITAN Xp GPU.

Fig. 4(b) shows that the time needed for anytime sampling increases almost linearly with respect to the sampled code length. This supports our argument in Section 3.2 that the run-time of decoding is

negligible compared to the autoregressive component. Indeed, the decoder took around 23 seconds to generate all samples for CelebA, whereas the sampling time of the autoregressive model was around 610 seconds—over an order of magnitude larger. Moreover, since we can achieve roughly the highest sample quality with only 60% of the full code length on CelebA, anytime sampling can save around 40% run-time compared to naïve sampling without hurting sample quality.

In addition, our method is faster than the original VQ-VAE even when sampling the full code length, without compromising sample quality (*cf*., Section 5.2.1). This is because the Transformer model we used is sufficiently shallower than the Gated PixelCNN (van den Oord et al., 2016) model in the original VQ-VAE paper. Compared to PixelCNN++ (Salimans et al., 2017), an autoregressive model on the raw pixel space, the sampling speed of our method can be an order of magnitude faster since our autoregressive models are trained on the latent space with much lower dimensionality.

6 Related Work

Prior work has tackled the issue of slow autoregressive generation by improving implementations of the generation algorithm. For example, the sampling speed of convolutional autoregressive models can be improved substantially by caching hidden state computation (Ramachandran et al., 2017). While such approaches provide substantial speedups in generation time, they are still at best linear in the dimension of the sample space. van den Oord et al. (2018) improves the inference speed by allowing parallel computing. Compared to our approach, they do not have the test-time adaptivity to computational constraints. In contrast, we design methods that allow trade-offs between generation speed and sample quality on the fly based on computational constraints, without model re-training. For example, running apps need to accommodate to the real-time computational resources without model re-training.

In order to enable anytime sampling, our method requires learning an ordered latent representation of data by training ordered autoencoders. A similar method for training ordered encoders was proposed in Rippel et al. (2014). Instead of uniform distribution over discrete codes in our method, they adopted a geometric distribution over continuous codes during the training of the ordered autoencoders. Because of the difference they require additional tricks such as unit sweeping and adaptive regularization coefficients to stabilize the training, while our training is stable and more suitable for large scale training. In addition, they only focus on fast retrieval and image compression. By contrast, we further extend our approach to autoencoders with discrete latent codes (*e.g*., VQ-VAEs) and explore their applications in anytime sampling for autoregressive models. Another work related to our approach is hierarchical nonlinear PCA (Scholz & Vigário, 2002). We generalize their approach to latent spaces of arbitrary dimensionality, and leverage Monte Carlo estimations to improve the efficiency when learning very high dimensional latent representations.

A line of works draw connections between PCA and the linear autoencoders. Kunin et al. (2019) prove that the principal directions can be deduced from the critical points of L_2 regularized linear autoencoders. Grover & Ermon (2019) show that the optimal measurement matrix recovers the principal components and Pfau et al. (2019) use deep neural network to approximate eigenfunctions of linear operators.

7 Conclusion

Sampling from autoregressive models is an expensive sequential process that can be intractable when on a tight computing budget. To address this difficulty, we consider the novel task of adaptive autoregressive sampling that can naturally trade-off computation with sample quality. Inspired by PCA, we adopt ordered autoencoders, whose latent codes are prioritized based on their importance to reconstruction. We show that it is possible to do anytime sampling for autoregressive models trained on these ordered latent codes—we may stop the sequential sampling process at any step and still obtain a complete sample of reasonable quality by decoding the partial codes.

With both theoretical arguments and empirical evidence, we show that ordered autoencoders can induce a valid ordering that facilitates anytime sampling. Experimentally, we test our approach on several image and audio datasets by pairing an ordered VQ-VAE (a powerful autoencoder architecture) and a Transformer (an expressive autoregressive model) on the latent space. We demonstrate that our samples suffer almost no loss of quality (as measured by FID scores) for images when using only 60% to 80% of all code dimensions, and the sample quality degrades gracefully as we gradually reduce the code length.

Broader Impact Statement

Generative models is a burgeoning research field with widespread implications for science and society. Our work addresses the computational bottleneck in using autoregressive generative models for data generation. Given the powerful expressive capabilities of autroegressive models, this aids many downstream applications and in particular those that are limited by computational constraints and require *fast, real-time data generation*.

Depending on the specific downstream usecase, the use of these models can have both positive and negative outcomes. For example, autoregressive models with anytime sampling can be incorporated in producing image/audio samples on-the-fly. However deepfake technology can take the advantage of it and lead to social engineering scams. Autoregressive models with anytime sampling can also be used for planning and reinforcement learning algorithms to enable real-time decision making in complex environments. This further provides avenues for deployment in autonomous embodied artificial intelligence systems, such as self-driving cars. On one hand, such systems can save lives in certain scenarios e.g., error due to humans paying less attention to other traffic while driving can be reduced. At the same time, the current systems are too brittle and susceptible to adversarial examples leading to unanticipated failure. Besides the aforementioned limitations of such systems, there are also ethical concerns in deploying autonomous systems, e.g., the trolley problem. Addressing the above concerns requires further research in providing robustness guarantees for such model-based decision making algorithms as well as close collaborations with researchers in socio-technical disciplines.

References

Bengio, Y., Léonard, N., and Courville, A. Estimating or propagating gradients through stochastic neurons for conditional computation. *arXiv preprint arXiv:1308.3432*, 2013.

Donahue, C., McAuley, J. J., and Puckette, M. Adversarial audio synthesis. In *ICLR*, 2018.

Ghosh, P., Sajjadi, M. S. M., Vergari, A., Black, M. J., and Schölkopf, B. From variational to deterministic autoencoders. *ArXiv*, abs/1903.12436, 2020.

Grover, A. and Ermon, S. Uncertainty autoencoders: Learning compressed representations via variational information maximization. *ArXiv*, abs/1812.10539, 2019.

Guo, P., Ni, X., Chen, X., and Ji, X. Fast pixelcnn: Based on network acceleration cache and partial generation network. *2017 International Symposium on Intelligent Signal Processing and Communication Systems (ISPACS)*, pp. 71–76, 2017.

Heusel, M., Ramsauer, H., Unterthiner, T., Nessler, B., and Hochreiter, S. Gans trained by a two time-scale update rule converge to a local nash equilibrium. In *NIPS*, 2017a.

Heusel, M., Ramsauer, H., Unterthiner, T., Nessler, B., and Hochreiter, S. Gans trained by a two time-scale update rule converge to a local nash equilibrium. In *Advances in neural information processing systems*, pp. 6626–6637, 2017b.

Kalchbrenner, N., Espeholt, L., Simonyan, K., Oord, A. v. d., Graves, A., and Kavukcuoglu, K. Neural machine translation in linear time. *arXiv preprint arXiv:1610.10099*, 2016.

Kalchbrenner, N., van den Oord, A., Simonyan, K., Danihelka, I., Vinyals, O., Graves, A., and Kavukcuoglu, K. Video pixel networks. In *Proceedings of the 34th International Conference on Machine Learning-Volume 70*, pp. 1771–1779. JMLR. org, 2017.

Kingma, D. P. and Welling, M. Auto-encoding variational bayes. In *International Conference on Learning Representations*, 2013.

Krizhevsky, A. Learning multiple layers of features from tiny images. 2009.

Kunin, D., Bloom, J. M., Goeva, A., and Seed, C. Loss landscapes of regularized linear autoencoders. *ArXiv*, abs/1901.08168, 2019.

Liu, Z., Luo, P., Wang, X., and Tang, X. Deep learning face attributes in the wild. *2015 IEEE International Conference on Computer Vision (ICCV)*, pp. 3730–3738, 2014.

Menick, J. and Kalchbrenner, N. Generating high fidelity images with subscale pixel networks and multidimensional upscaling. *arXiv preprint arXiv:1812.01608*, 2018.

Oord, A. v. d., Dieleman, S., Zen, H., Simonyan, K., Vinyals, O., Graves, A., Kalchbrenner, N., Senior, A., and Kavukcuoglu, K. Wavenet: A generative model for raw audio. *arXiv preprint arXiv:1609.03499*, 2016a.

Oord, A. v. d., Kalchbrenner, N., and Kavukcuoglu, K. Pixel recurrent neural networks. *arXiv preprint arXiv:1601.06759*, 2016b.

Papamakarios, G., Pavlakou, T., and Murray, I. Masked autoregressive flow for density estimation. In *Advances in Neural Information Processing Systems*, pp. 2338–2347, 2017.

Pfau, D., Petersen, S., Agarwal, A., Barrett, D. G. T., and Stachenfeld, K. L. Spectral inference networks: Unifying deep and spectral learning. In *ICLR*, 2019.

Radford, A., Wu, J., Child, R., Luan, D., Amodei, D., and Sutskever, I. Language models are unsupervised multitask learners. *OpenAI Blog*, 1(8):9, 2019.

Ramachandran, P., Paine, T. L., Khorrami, P., Babaeizadeh, M., Chang, S., Zhang, Y., Hasegawa-Johnson, M. A., Campbell, R. H., and Huang, T. S. Fast generation for convolutional autoregressive models. *ArXiv*, abs/1704.06001, 2017.

Razavi, A., van den Oord, A., and Vinyals, O. Generating diverse high-fidelity images with vq-vae-2. In *Advances in Neural Information Processing Systems*, pp. 14837–14847, 2019.

Rippel, O., Gelbart, M. A., and Adams, R. P. Learning ordered representations with nested dropout. In *ICML*, 2014.

Salimans, T., Karpathy, A., Chen, X., and Kingma, D. P. Pixelcnn++: Improving the pixelcnn with discretized logistic mixture likelihood and other modifications. *arXiv preprint arXiv:1701.05517*, 2017.

Scholz, M. and Vigário, R. Nonlinear pca: a new hierarchical approach. In *ESANN*, 2002.

van den Oord, A., Kalchbrenner, N., Espeholt, L., Kavukcuoglu, K., Vinyals, O., and Graves, A. Conditional image generation with pixelcnn decoders. In *NIPS*, 2016.

van den Oord, A., Vinyals, O., and Kavukcuoglu, K. Neural discrete representation learning. In *NIPS*, 2017.

van den Oord, A., Li, Y., Babuschkin, I., Simonyan, K., Vinyals, O., Kavukcuoglu, K., van den Driessche, G., Lockhart, E., Cobo, L. C., Stimberg, F., Casagrande, N., Grewe, D., Noury, S., Dieleman, S., Elsen, E., Kalchbrenner, N., Zen, H., Graves, A., King, H., Walters, T., Belov, D., and Hassabis, D. Parallel wavenet: Fast high-fidelity speech synthesis. *ArXiv*, abs/1711.10433, 2018.

Vaswani, A., Shazeer, N., Parmar, N., Uszkoreit, J., Jones, L., Gomez, A. N., Kaiser, Ł., and Polosukhin, I. Attention is all you need. In *Advances in neural information processing systems*, pp. 5998–6008, 2017.

Veaux, C., Yamagishi, J., and Macdonald, K. Cstr vctk corpus: English multi-speaker corpus for cstr voice cloning toolkit. 2017.